Annals of Hepatology 30 (2025) 101897

Contents lists available at ScienceDirect

Annals of Hepatology

journal homepage: www.elsevier.es/annalsofhepatology

Original article

Naringenin attenuates early hepatocarcinogenesis induced by a MASH model

Linda Vanessa Márquez-Quiroga[a], Aline Barboza-López[a], Jose Y. Suárez-Castillo[a], Irina Cardoso-Lezama[a], Miguel Á. Fuentes-Figueroa[b], Eduardo E. Vargas-Pozada[a], Juan D. Rodriguez-Callejas[c], Erika Ramos-Tovar[d], Carolina Piña-Vázquez[e], Jaime Arellanes-Robledo[f,g], Saúl Villa-Treviño[e], Pablo Muriel[a,*]

[a] *Laboratorio de Hepatología Experimental, Departamento de Farmacología, Centro de Investigación y de Estudios Avanzados del IPN (CINVESTAV-IPN),* Av. *Instituto Politécnico Nacional, No 2508 Col. San Pedro Zacatenco, CDMX, C.P. 07360, Mexico*
[b] *Laboratorio de Biología Celular y Productos Naturales, Escuela Nacional de Medicina y Homeopatía-IPN, Guillermo Massieu Helguera, La Escalera, CDMX, C.P. 07320, Mexico*
[c] *Servicio de Geriatría, Instituto Nacional de Ciencias Médicas y Nutrición Salvador Zubirán, Vasco de Quiroga 15, Belisario Dominguez Secc 16, Tlalpan, CDMX, C.P. 14080, Mexico*
[d] *Sección de Estudios de Posgrado e Investigación, Escuela Superior de Medicina-IPN, Plan de San Luis y Díaz Mirón s/n, Casco de Santo Tomas, CDMX, C.P. 11340, Mexico*
[e] *Departamento de Biología Celular, CINVESTAV-IPN,* Av. *Instituto Politécnico Nacional, No 2508 Col. San Pedro Zacatenco, CDMX, C.P. 07360, Mexico*
[f] *Laboratorio de Enfermedades Hepáticas, Instituto Nacional de Medicina Genómica – INMEGEN, CDMX, C.P. 14610, Mexico*
[g] *Subdirección de Investigaciones Humanísticas y Científicas, Consejo Nacional de Humanidades, Ciencias y Tecnologías, CONAHCYT, CDMX, C.P. 03940 Mexico*

ARTICLE INFO

Article History:
Received 15 November 2024
Accepted 13 February 2025
Available online 19 March 2025

Keywords:
Nonalcoholic fatty liver disease
Nonalcoholic steatohepatitis
Fibrosis
Preneoplastic lesion
Flavonoid

ABSTRACT

Introduction and Objectives: Nucleotide-binding oligomerization domain-like receptor family pyrin domain-containing 3 (NLRP3) inflammasome plays a critical role in the progression of metabolic dysfunction-associated steatohepatitis (MASH). Here, we investigated the effects of naringenin (NAR) on early hepatocellular carcinoma (HCC) experimentally induced in a rat MASH model and whether the NLRP3 inflammasome/pyroptosis pathway was involved.
Materials and Methods: The animals were fed a hepatopathogenic diet for 16 weeks and carbon tetrachloride (400 mg/kg, i.p.) and diethylnitrosamine (40 mg/kg, *i.p.*) were injected once a week. NAR was administered at 100 mg/kg *p.o.* The effects of NAR on the MASH—HCC protocol were evaluated using biochemical, histological, *in silico*, and molecular biological approaches.
Results: NAR significantly mitigated liver damage, as evidenced by the reduction in liver damage markers. It also reduced steatosis and inflammation, as determined by decreased lipid accumulation and sterol regulatory element-binding protein 1C, interleukins 1-beta and 18, and nuclear factor kappa B levels, and also increased peroxisome proliferator-activated receptor gamma levels. NAR inhibits the formation of NLRP3, including the recruitment of caspase-1 and gasdermin D proteins, and reduces the levels of transforming growth factor-beta, alpha-smooth muscle actin, and hepatic collagen 1, thereby diminishing extracellular matrix synthesis. Furthermore, gamma-glutamyl transpeptidase activity, glutathione S-transferase pi 1, and the proliferation marker KI67 were considerably reduced.

Abbreviations: ALT, Alanine aminotransferase; AP, alkaline phosphatase; BW, body weight; CCl_4, carbon tetrachloride; CTL, control; DAMPs, damage-associated molecular patterns; DAPI, 4′,6′-diamidino-2-phenylindole, dihydrochloride; DEN, diethylnitrosamine; ECM, extracellular matrix; GGT, gamma-glutamyl transpeptidase; H&E, hematoxylin and eosin; HSC, hepatic stellate cells; HCC, hepatocellular carcinoma; IF, immunofluorescence; IHC, immunohistochemical; NAR, naringenin; NAFLD, non-alcoholic fatty liver disease; NASH, non-alcoholic steatohepatitis; MASLD, metabolic dysfunction-associated steatotic liver disease; MASH, metabolic dysfunction-associated steatohepatitis; M-HCC, MASH-driven HCC; ORO, oil red "O"; PAMPs, pathogen-associated molecular patterns; SEM, standard error of the mean; α-SMA, Symbols: alpha-smooth muscle actin; ASC, apoptosis-associated speck-like protein containing a CARD; BCL-2, B-cell lymphoma 2; ChREBP, carbohydrate-responsive element-binding protein; GSDMD, gasdermin D; GSTP1, glutathione S-transferase pi 1; IL-18, interleukin-18; IL-1β, interleukin-1β; NF-κB, nuclear factor-κB; Nrf2, nuclear factor erythroid 2-related factor 2; NLRP3, nucleotide-binding oligomerization domain-like receptor family pyrin domain-containing 3; PPAR-γ, peroxisome proliferator-activated receptor gamma; P2$\times$7R, purinergic receptor; SREBP-1c, sterol regulatory element-binding protein 1C; TXNIP, thioredoxin interacting protein; TGF-β, transforming growth factor-beta

* Corresponding author.
E-mail address: pmuriel@cinvestav.mx (P. Muriel).

https://doi.org/10.1016/j.aohep.2025.101897

Conclusions: Our findings show that NAR has the potential to inhibit early HCC induced in the context of MASH, thereby suggesting that NAR could be used for MASH treatment in humans.

1. Introduction

Nonalcoholic fatty liver disease (NAFLD), now redefined as metabolic dysfunction-associated steatotic liver disease (MASLD), is a benign disease characterized by triglyceride build-up in liver cells (>5 %) resulting from complex interactions with various cardiometabolic risk factors [1,2]. Recent epidemiological studies estimate that MASLD affects >30 % of the global population, with a prevalence of 44 % in Latin America [3,4]. This disease encompasses simple fat accumulation to metabolic dysfunction-associated steatohepatitis (MASH), formerly known as nonalcoholic steatohepatitis (NASH), which is characterized by macrovesicular steatosis, lobular inflammation, and may progress to cirrhosis and hepatocellular carcinoma (HCC) [2,3,5].

MASH—HCC progression is promoted by inflammation, which leads to chronic hepatocyte cell death and compensatory proliferation during MASH bearing mild to advanced fibrosis and increased levels of transforming growth factor-β (TGF-β), interleukin-1β (IL-1β), interleukin-18 (IL-18), as well as activation of hepatic stellate cells (HSCs) and liver sinusoidal endothelial cells, which contribute to chromosomal aberrations and consequently promote HCC development [6–8].

Recently, it has been shown that inflammasomes play a crucial role in both innate immune and non-immune cell responses, such as those of neutrophils and hepatocytes, respectively, thereby promoting a chronic inflammatory environment that serves as a signaling platform that is activated in response to excessive pathogenic and cellular stress-related products in the liver [9,11]. The nucleotide-binding oligomerization domain-like receptor family pyrin domain-containing 3 (NLRP3) inflammasome is the most extensively studied and well characterized; it consists of NLRP3, an apoptosis-associated speck-like protein containing CARD (ASC), and pro-caspase-1 [9]. Activation of NLRP3 inflammasome complex leads to caspase-1 activation, which triggers IL-1β and IL-18 maturation and pyroptosis [9,11].

Pyroptosis is a highly inflammatory process characterized by gasdermin D (GSDMD) synthesis mediated by caspase-1 to form rapid cell swelling, pores in the plasma membrane, and release of intracellular pro-inflammatory proteins, such as IL-1β and IL-18, as well as NLRP3 and TGF-β, which might amplify inflammation and contribute to tissue damage [8,9]. Pyroptosis may be involved in several HCC mechanisms mediated by MASH such as tumor microenvironment promotion through the release of IL-1β and IL-18, and damage-associated molecular patterns (DAMPs) produced lipid accumulation and oxidative stress, two hallmarks of MASH, resulting in chronic liver inflammation that leads to DNA damage [8–10]. Moreover, pyroptosis-induced inflammation stimulates HSC activation and collagen production, thereby stimulating a profibrotic microenvironment and activating pro-tumorigenic signaling pathways [10,11].

This evidence strongly suggests that the NLRP3 inflammasome/-pyroptosis pathway is an attractive therapeutic target in MASH-driven HCC. In contrast, evidence also indicates that naringenin (NAR), a flavonoid found in various citrus fruits such as oranges, grapefruits, and lemons, has antioxidant, anti-inflammatory, and anticancer properties and inhibits the NLRP3/pyroptosis pathway [12–15].

It has been shown that the antioxidant effects of NAR are closely associated with the activation of the nuclear factor erythroid 2-related factor 2 pathway and regulation of antioxidant and detoxification gene expression [15]. Consequently, NAR enhances cellular antioxidant defense, reduces oxidative stress, and inhibits inflammation, thereby protecting liver cells from damage [15].

Although the effect of NAR on suppressing the NLRP3 inflammasome/pyroptosis pathway mediated by either MASH or HCC has been investigated [14,15], its anticancer activity in the MASH-driven HCC microenvironment remains unexplored. Thus, we aimed to assess the effect of NAR on early HCC induced by a MASH—HCC model and determine whether this flavonoid exerts its anticancer effect by regulating the NLRP3 inflammasome/pyroptosis pathway.

2. Materials and Methods

2.1. Experimental design

Six-week-old male Fischer 344 rats weighing 100–120 g (n = 20) were sourced from the Laboratory of Animal Production and Experimentation Unit at the Center for Research and Advanced Studies of the National Polytechnic Institute (UPEAL-CINVESTAV-IPN; CDMX, Mexico). All experimental procedures were performed according to the institutional guidelines approved by the Ethics Committee of CINVESTAV-IPN under protocol No. 310–20 and in line with Mexican official regulations (NOM-062-ZOO-1999). Animals were housed in a room with regulated conditions of 21 ± 1 °C, 50–60 % relative humidity, a 12-hour dark/night cycle, and unrestricted access to both water and food. Before the experiment, the rats were acclimatized for one week.

Animals were randomly divided into four groups (n = 5 per group). Control (CTL) and NAR groups were fed a standard diet ad libitum (5053, Labdiet, Brentwood, MO, USA) for 16 weeks (Fig. 1). The CTL group received 14 and 10 weekly injections of liquid petrolatum (7110; Reactivos Química Meyer. Mexico City, CDMX, MX) and Milli-Q water were vehicles for carbon tetrachloride (CCl_4, 31,996–1, Merck-Millipore Burlington, MA, USA) and diethylnitrosamine (DEN, N0756, Merck-Millipore. Burlington, MA, USA), respectively (Fig. 1). To develop a MASH-driven HCC (M-HCC) model, animals were fed a hepatopathogenic diet (Table 1) for 16 weeks and intraperitoneally (i.p.) injected with CCl_4 at 400 mg/kg body weight (BW) and DEN at 40 mg/kg BW once a week for 14 and 10 weeks, respectively [8,16–18]. The CCl_4 administration protocol was previously described by Cardoso-Lezama I, *et al.* [8], Vargas-Pozada EE, *et al.* [17], and Vargas-Pozada EE, *et al.* [18], and the DEN protocol was adapted from the hepatocarcinogenesis model previously described by Shiffer E, *et al.* [19]. DEN administration was initiated seven weeks after the onset of the high cholesterol diet, as shown in Fig. 1. A group of animals subjected to either NAR alone or M-HCC + NAR was administered NAR daily by gavage (W530098; Merck-Millipore. Burlington, MA, USA) at 100 mg/kg BW and suspended in 0.7 % carboxymethyl cellulose [12] (5895–1000, Reactivos Química Meyer. Mexico City, CDMX, and MX, respectively) for 16 weeks (Fig. 1). One week after NAR administration, namely at 17 weeks, the rats were euthanized by exsanguination following an intraperitoneal injection of a mixture of ketamine at 100 mg/kg BW (A028062, Anesket PiSA, Zapopan, JAL, MX) and xylazine at 8 mg/kg BW (A114218, Procin PiSA, Zapopan, JAL, MX).

2.2. Biochemical measurements

Blood samples were obtained by intracardiac puncture and centrifuged at 3000 rpm for 15 min. To determine liver damage, serum activities of alanine aminotransferase (ALT), alkaline phosphatase (AP), and γ-glutamyl transpeptidase (GGT) were measured by colorimetric methods [20–22]. Hepatic glycogen content was quantified in

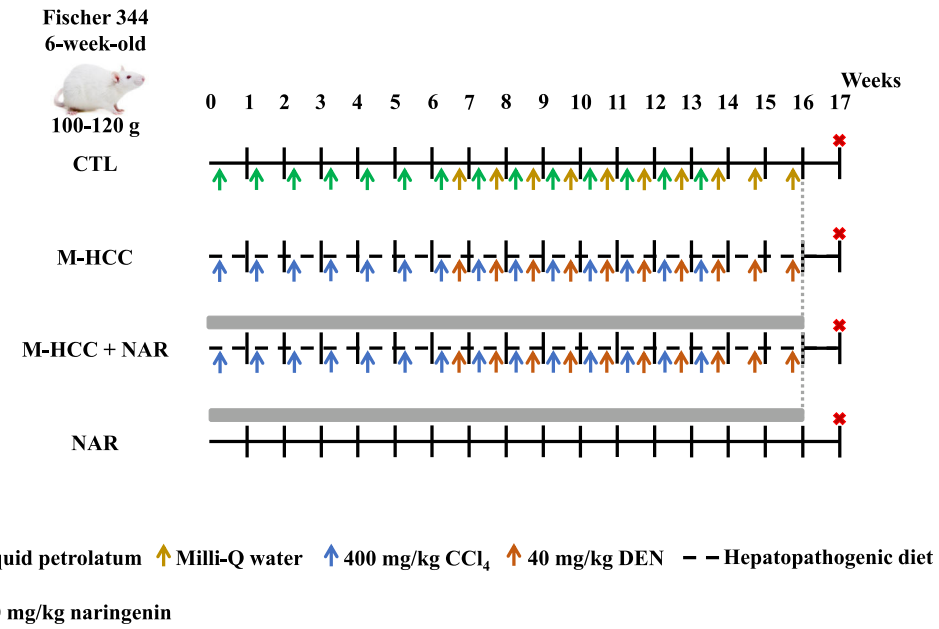

Fig. 1. Schematic representation of M-HCC and NAR administration.

The control (CTL) group was fed ad libitum a standard diet, illustrated with a continuous black line, along with weekly i.p. injections of liquid petrolatum (depicted with green arrows) and Milli-Q water (indicated by golden arrows). MASH-driven HCC (M-HCC) + naringenin (NAR) group received daily NAR at 100 mg/kg by gavage (illustrated with a continuous grey line). The NAR group received the standard diet and NAR at 100 mg/kg by gavage. Experimental groups had unrestricted access to a hepatopathogenic diet for 16 weeks, shown by a black dashed line, and CCl4 at 400 mg/kg, marked by blue arrows. In the last 10 weeks, DEN was administered at 40 mg/kg via i.p. injection, represented with orange arrows. Euthanasia of animals is indicated in red asterisks. CTL, control; M-HCC, MASH-driven HCC; NAR, naringenin; M-HCC+NAR, MASH-driven HCC administrated with naringenin. *n* = 5 animals per group.

Table 1
Hepatopathogenic diet.

Ingredients	%	Catalog	Brand
Casein	10	–	Irish Dairy Board, Dublin, IE
Cholate	0.5	C1254	Merck-Millipore. Burlington, MA, USA
Cholesterol	1	C8667	Merck-Millipore. Burlington, MA, USA
Icing sugar	30	–	Zulka (Zucarmex S.A. de C.V., Culiacán, SIN, MX)
Unsalted butter	5	–	Gloria (Cremería Americana S.A. de C.V., Mexico City, CMX, MX Mexico)
Standard 5053 diet	53.5	5053	Labdiet, Brentwood, MO, USA

fresh liver samples using the anthrone method [23]. Finally, absorbance measurements were performed at 515 nm for ALT, 410 nm for AP and GGT, and 620 nm for glycogen. Milli-Q water was used as a reference blank, and measurements were obtained using a SHIMADZU UV-1201 spectrophotometer (Shimadzu Corporation, Kyoto, JPN).

2.3. Western blot analysis

For the extraction of total proteins, tissue samples were prepared in a buffer containing a Protease Inhibitor Cocktail and phosphatase inhibitors (P8340 and P0044, respectively, Merck-Millipore Burlington, MA, USA) and quantified using the bicinchoninic acid method [24,25]. Membranes were then incubated with the primary and secondary antibodies of interest (Table 2) and detected using Immobilon Forte Western HRP substrate (WBLUF0100; Merck-Millipore. Burlington, MA, USA). Protein levels were normalized by re-probing the blots against GAPDH levels. For quantitative analysis, densitometry was performed using the ImageJ® software, version 1.53t (National Institutes of Health, Bethesda, MD, USA).

Table 2
Antibodies for immunohistochemistry (IHC), western blot, and immunofluorescence (IF) Analyses.

Protein	IHC dilution	WB dilution	IF dilution	Catalog	Brand
IL-1β	1:100			AB18329	Abcam (Cambridge, MA, USA)
IL-18	1:100			A16737	Cell Signaling Technology (Danvers, MA, USA)
PPAR-γ		1:500		SC-398,394	Santa Cruz Biotechnology (Santa Cruz, CA, USA)
SREB-1C		1:500		AB28481	Abcam (Cambridge, MA, USA)
p-65		1:500		MAB3026	Merck-Millipore (Burlington, MA, USA)
NLRP3	1:100	1:500	1:250	NBP2−12,446	Novus Biologicals (Littleton, CO, USA)
Pro caspase-1		1:500		SC-392,736	Santa Cruz Biotechnology (Santa Cruz, CA, USA)
Caspase-1	1:100	1:500		SC-392,736	Santa Cruz Biotechnology (Santa Cruz, CA, USA)
GSDMD	1:100	1:500	1:250	SC-393,581	Santa Cruz Biotechnology (Santa Cruz, CA, USA)
TGF-β		1:500		MAB1032	Merck-Millipore (Burlington, MA, USA)
α-SMA		1:500		A-5691	Merck-Millipore (Burlington, MA, USA)
Ki-67	1:10			MAB1032	Merck-Millipore (Burlington, MA, USA)
GSTP1	1:100	1:500		A-5691	Merck-Millipore (Burlington, MA, USA)

Table 3
Molecular docking of NAR with proteins associated with NLRP3 inflammasome/pyroptosis pathway.

Protein	PDB ID	Vina Score	Center (x, y, z)	Size (x, y, z)	Interactions
p65	6YPY	−7.2	18.75, 22.49, −0.17	15,15,15	ASP215; LEU218; ILE219; LYS122; ILE46; GLY48
NLRP3	7ALV	−5.8	16.80, 35.36, 125.70	15,15,15	TYR443; ILE411; ALA227; ARG578; TYR632; ASP662
ASC	2KN6	−4.3	−15, 0.1, −13	17,17,17	PHE163; LEU192; LEU178; LYS174
Caspase-1	1RWK	−6.5	33.09, 60.69, 4.87	15,15,15	GLY238; HIS237; ARG179; GLN283; ALA284; ARG341; CYS285
IL-1β	1ITB	−6.6	30, −2, 7	15,15,15	TYR24; LEU82; LEU80; PRO78
IL-18	3F62	−2.9	5.3, 10.2, 12	15,15,15	ARG104; GLU116; GLN114
GSDMD	5WQT	−6.7	29.14, −94.17, 44.25	26,26,26	LEU49; PRO73; ASP47; ALA53
P2×7R	4NTJ	−8.3	17, 101.02, 50.65	15,15,15	ARG256; GLN195; TYR105; ASN191; VAL102; VAL190; CYS194; ASN159; PHE106; SER156
TXNIP	4GEI	−6.6	17, 39, −8	19,19,19	TYR99; VAL89; ALA43; GLU85
ChREBP	6YGJ	−6.6	4.89, −38.80, 20.51	15,15,15	LEU174; ARG128; ARG129; ARG58; TRP127

2.4. Staining of hematoxylin & eosin (H&E) and Masson's trichrome, and immunohistochemistry (IHC) analysis

Liver tissues were fixed in 4 % paraformaldehyde (00,380; Polyscience. Warrington, PA, USA) dissolved in 1X PBS, for 24 h, and embedded in paraffin. Then, samples were cut into 3 μm thick slices, mounted on electrocharged glass slides, deparaffined, dehydrated, and processed by H&E and Masson's stains, following standard protocols [26]. For IHC, after rehydration, antigens were unmasked in 0.01 M sodium citrate buffer (pH 6.0) for 20 min at 120 °C and washed with 1X PBS for 5 min. Endogenous peroxidase activity and nonspecific protein binding were blocked using 8 % H_2O_2 (2186–01, JT Baker. New Jersey, WA, USA) and 10 % nonfat milk for 1 h each. Afterward, tissue slices were incubated with primary antibodies overnight at 4 °C (Table 2). The proteins of interest were detected using secondary antibodies (Table 2) and incubated for 2 h at room temperature. Staining was examined under a bright-field microscope (Olympus IX70; Olympus

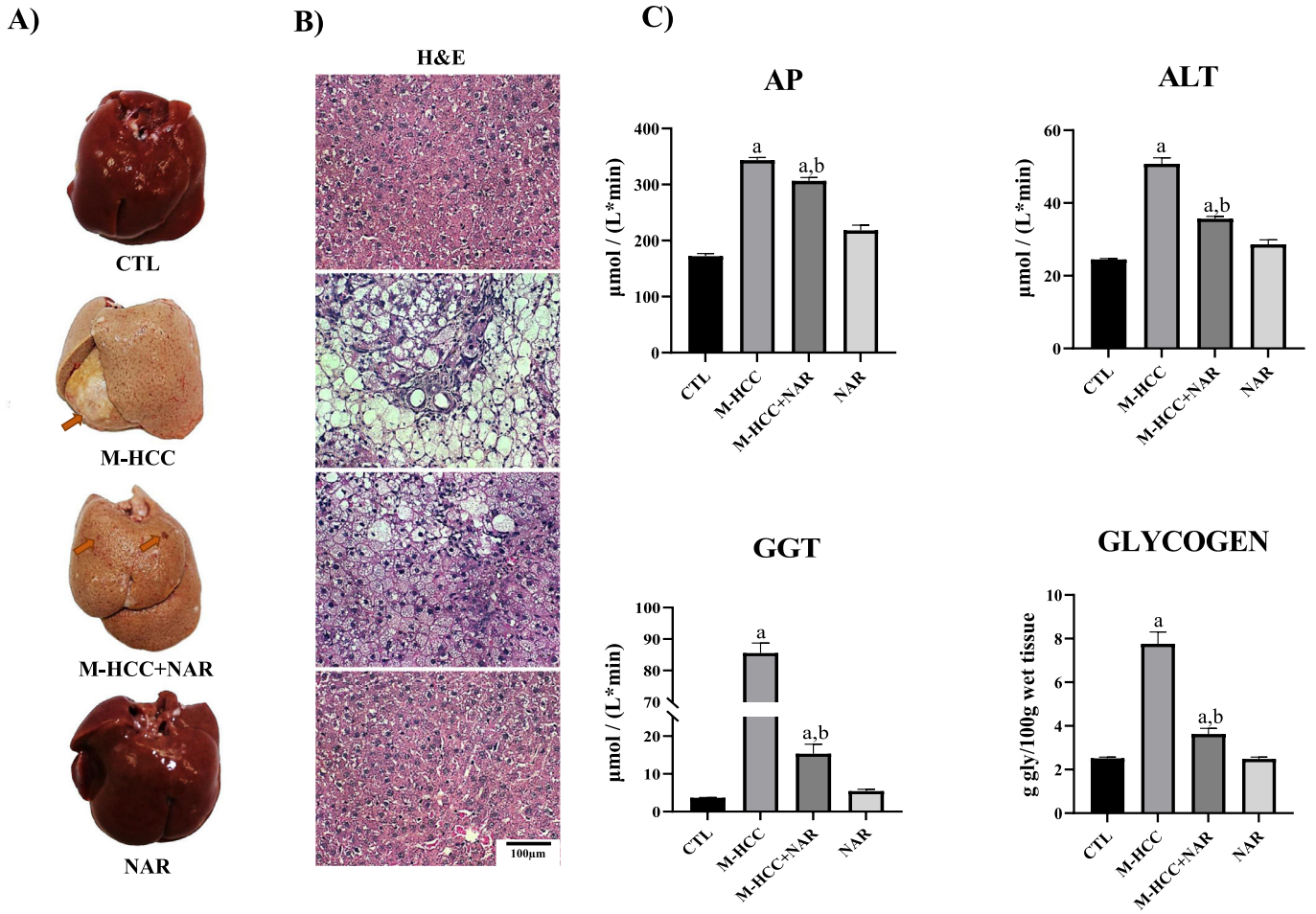

Fig. 2. Effect of NAR on liver structure, cellular damage, and glycogen levels in the MASH—HCC model.
(A) Representative macroscopic images of livers from each experimental group. **(B)** Microscopic images of liver tissue sections stained with H&E. **(C)** Markers of liver damage. Serum activity of AP, ALT, GGT, and hepatic glycogen content. In plots, bars represent the mean ± SEM obtained by two-way ANOVA statistical analysis. Statistically significant when compared with CTL (a) and M-HCC (b) groups; $p < 0.05$. CTL, control; M-HCC, MASH-driven HCC; NAR, naringenin; M-HCC+NAR, MASH-driven HCC administrated with naringenin. $n = 5$ animals per group.

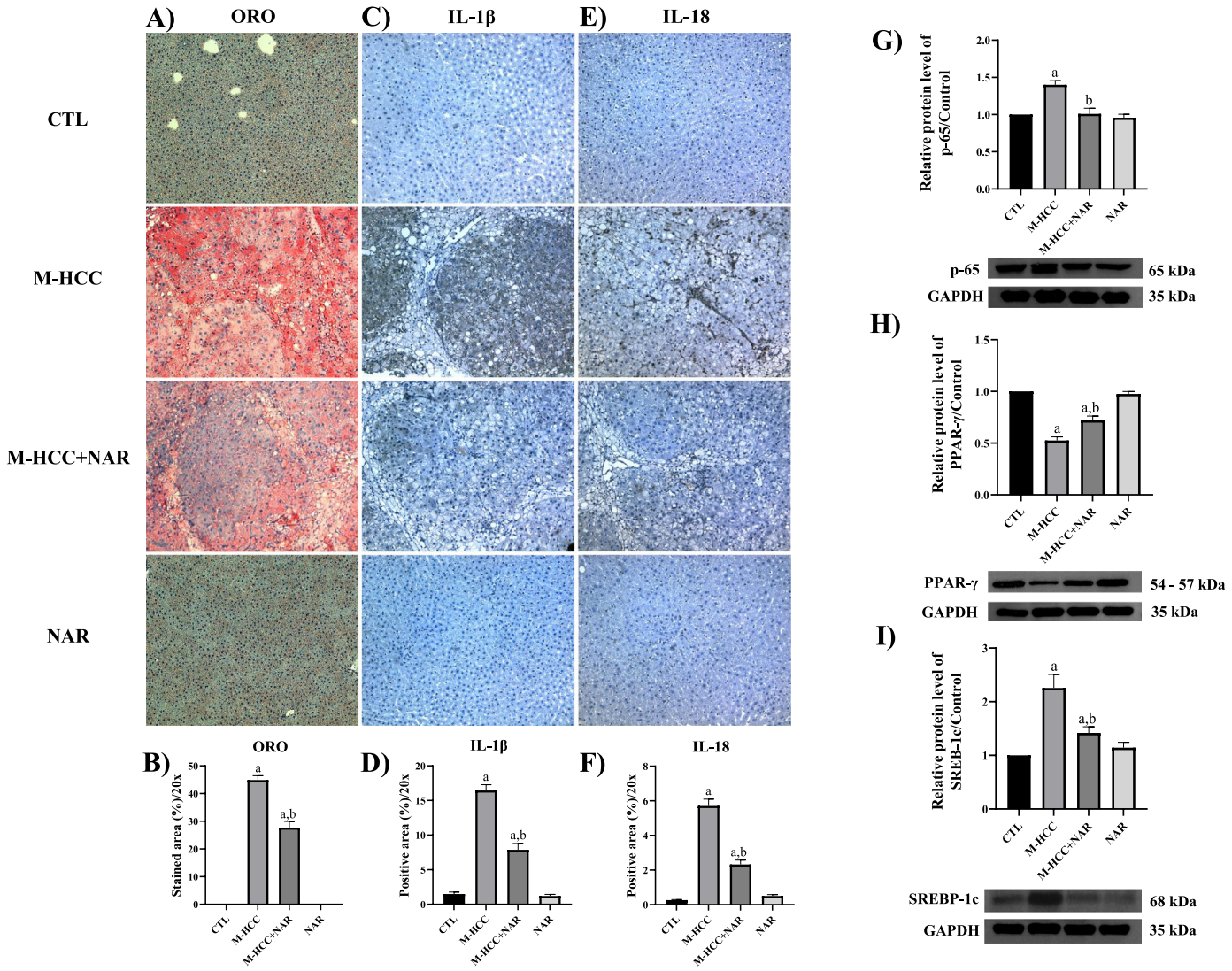

Fig. 3. Effect of NAR on lipid accumulation, steatosis markers, and pro-inflammatory protein production.

(A) Representative images of liver tissue-stained ORO and IHC staining of IL-1β and IL-18 proteins. Quantification of ORO-positive area **(B)**, IL-1β **(C)**, and IL-18 **(D)** Determination of protein levels by Western blotting of PPAR-γ **(E)**, SREBP-1C **(F)**, and p65 **(G)**. In plots, bars represent the mean ± SEM obtained by two-way ANOVA statistical analysis. Statistically significant when compared with CTL (a) and M-HCC (b) groups; $p < 0.05$. CTL, control; M-HCC, MASH-driven HCC; NAR, naringenin; M-HCC+NAR, MASH-driven HCC administrated with naringenin. $n = 3$ animals per group.

Corporation. Hachioji, Tokyo, JP). The acquired images were examined utilizing the ImageJ® software, version 1.53t (National Institutes of Health, Bethesda, MD, USA).

2.5. Immunofluorescence (IF) staining

IF staining was performed on tissue slices using a double-labeling procedure to detect both NLRP3 and GSDMD proteins following previously established protocols [27,28]. Sections were incubated at 4 °C overnight with primary antibodies and then with secondary antibodies (Table 2) in 0.2 % PBS-Tween for 2 h at room temperature. Label detection and image capture were performed by confocal microscopy using a Leica TCS SP8 AOBS DMI6000 confocal microscope (Acousto-optical Beam Splitter, Wetzlar, HE, USA).

2.6. Oil red O (ORO) staining and GGT activity

Frozen liver tissues were cut into 8 and 20-thick slices, affixed in glass slides coated with poly-L-lysine (P8920, Merck-Millipore. Burlington, MA, USA) and processed for ORO and GGT staining [29]. The ORO staining images were captured using an Olympus IX70 bright-field microscope (Olympus Corporation, Tokyo, JPN) and examined using ImageJ software, version 1.53t (National Institutes of Health, Bethesda, MD, USA). GGT-positive foci were captured and quantified using the AnalySIS Opty Soft Imaging System GmbH 3.00 software (Olympus Corporation, Hachioji, Tokyo, JPN).

2.7. Molecular docking

The starting point for ligand preparation involved the minimum-energy molecular model for (*S*)-naringenin NAR from X-ray diffraction [30] in Chem3D 20.0 and energy minimization using MM2 (PerkinElmer Inc, Waltham, MA, USA) conformational search using MMFF94 force field (Spartan 14, wavefunction Inc., Irvine, CA, USA), energy calculation using DFT at B3LYP/6−31g(d) level, and geometry optimization at B3LYP/DGDZVP level of theory (Gaussian 03, Gaussian Inc., Wallingford, CT, USA). Crystal structures of various proteins, including nuclear factor-κB (NF-κB) (6YPY), NLRP3 (7ALV), ASC

Table 4
NAFLD activity score (NAS).

Groups	Steatosis	Lobular inflammation	Ballooning	NAS
CTL	0.0 (0.0)	0.0 (0.0)	0.0 (0.0)	0.0 (0.0)
M-HCC	2.0 (0.0) [a]	2.2 (0.2) [a]	2.0 (0.0) [a]	6.2 (0.2) [a]
M-HCC+NAR	1.0 (0.0) [b]	1.1 (0.1) [b]	1.4 (0.2) [b]	3.5 (0.2) [b]
NAR	0.0 (0.0)	0.0 (0.0)	0.0 (0.0)	0.0 (0.0)

Results were expressed as mean ± SEM and were obtained by two-way ANOVA statistical analysis. Statistically significant when compared with CTL (a) and M-HCC (b) groups; $p < 0.05$. CTL, control; M-HCC, MASH-driven HCC; NAR, naringenin; M-HCC +NAR, MASH-driven HCC administrated with NAR.

(2KN6), caspase-1 (1RWK), IL-1β (1ITB), IL-18 (3F62), GSDMD (5WQT), purinergic receptor (P2×7R) (4NTJ), carbohydrate-responsive element-binding protein (ChREBP) (6YGJ) and thioredoxin interacting protein (TXNIP) (4GEI), were retrieved from the RCSB Protein Data Bank (Table 3). Docking procedures were carried out using AutoDock Tools 4.2 (The Scripps Research Institute, La Jolla, CA, USA) on a computer system equipped with an AMD Ryzen 7 processor operating at 1.80 GHz with Radeon Graphics and 16 GB of RAM. Subsequently, the results were analyzed using AutoDock Tools 4.2, PyMOL 2.1 (Schrödinger), and BIOVIA Discovery Studio 2018 (BIOVIA, San Diego, CA, USA) software tailored for the Windows operating system.

2.8. Statistical analysis

The data are presented as mean values ± *S*.E.M. Statistical analyses were conducted using two-way ANOVA followed by Tukey's post hoc test. The significance level was set at $p < 0.05$. Statistical analyses were performed using GraphPad Software, version 8.0.1 (244) (GraphPad, La Jolla, CA, USA).

2.9. Ethical statements

All experimental procedures were performed according to the institutional guidelines approved by the Ethics Committee of CINVESTAV-IPN under protocol No. 310−20 and in line with Mexican official regulations (NOM-062-ZOO-1999). All animal experiments complied with the ARRIVE guidelines and were carried out following the U.K. Animals (Scientific Procedures) Act, 1986 and associated guidelines, EU Directive 2010/63/EU for animal experiments, or the National Institutes of Health guide for the care and use of Laboratory animals (NIH Publications No. 8023, revised 1978). Male Fischer 344 rats were used in all experiments.

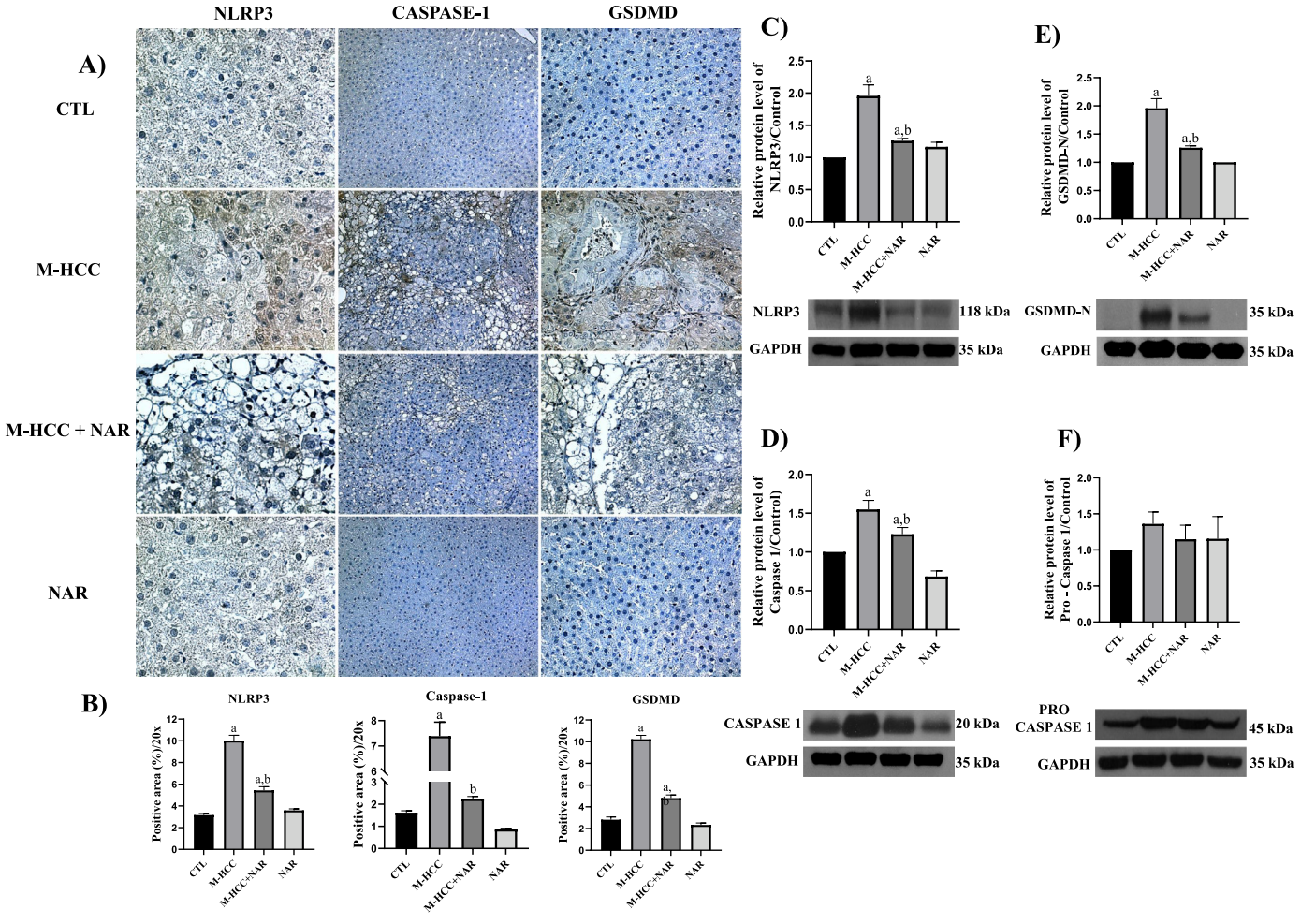

Fig. 4. Effect of NAR on NLRP3 inflammasome/pyroptosis pathway.
(A) IHC analysis of NLRP3, caspase-1, and GSDMD proteins. **(B)** Quantification of the positive area for NLRP3, caspase-1, and GSDMD proteins. Western blot analysis of NLRP3 **(C)**, pro-caspase-1 **(D)**, caspase-1 **(E)**, and GSDMD-N **(F)** proteins. In plots, bars represent the mean ± SEM obtained by two-way ANOVA statistical analysis. Statistically significant when compared with CTL (a) and M-HCC (b) groups; $p < 0.05$. control; M-HCC, MASH-driven HCC; NAR, naringenin; M-HCC+NAR, MASH-driven HCC administrated with naringenin. $n = 3$ animals per group.

3. Results

3.1. NAR attenuates liver damage in the MASH-driven HCC model

Fig. 2 shows images of the macroscopic and microscopic alterations in the liver tissues of animals in the MASH—HCC model and treated with NAR. Macroscopically (Fig. 2a), the liver from the control and NAR groups showed an unaltered classical bright red color, but that from the M-HCC group displayed a yellowish-white color and 83 % of the rats group showed visible tumors; interestingly, the liver from the M-HCC + NAR group exhibited a partial reduction in the appearance and only preneoplastic lesions were observed (Fig. 2a). The incidence of hepatic tumors was 83 % in the M-HCC group and 0 % in the M-HCC+NAR group ($p < 0.05$). The average number of tumors per liver was 1.0 ± 0.0 in the M-HCC group, which was significantly reduced to 0 ± 0 in the M-HCC+NAR group ($p < 0.01$).

Microscopically (Fig. 2b), the livers from the control and NAR groups exhibited normal polyhedral hepatocytes with central nuclei and eosinophilic cytoplasm, whereas from the M-HCC group showed disruption of the hepatic parenchyma, hepatocyte ballooning degeneration with peripheral nuclei, loss of cytoplasmic eosin, diffuse microvesicular and macrovesicular steatosis, inflammatory cell infiltration, necrosis, and altered hepatocyte foci. Notably, livers from the M-HCC + NAR group showed a significant reduction in the above alterations (Fig. 2b).

Histological alterations in the livers of the M-HCC group were accompanied by increased ($p = 0.0001$) serum levels of liver damage markers, such as AP, GGT, and ALT, compared to those in control rats. Conversely, NAR significantly reduced the activity of these enzymes (AP, $p = 0.005$; GGT and ALT, $p = 0.0001$) in the livers of animals subjected to M-HCC (Fig. 2c). Interestingly, the glycogen content was markedly reduced ($p = 0.0001$) by NAR in the livers of M-HCC rats (Fig. 2c). None of these liver injury markers were affected in either the control or NAR-treated groups (Fig. 2c).

3.2. NAR attenuates steatosis and pro-inflammatory markers

Animals subjected to the M-HCC model showed remarkable steatosis, characterized by copious lipid vesicles in the cytosol of hepatocytes (Fig. 3a), which was significantly decreased ($p = 0.0001$) by NAR treatment (Fig. 3b). The NAFLD activity score (NAS) is shown in Table 4.

The proteins involved in inflammation, such as IL-1β, IL-18, and p65, were evaluated by IHC and western blot (Fig. 3c,d,e,f,g). Animals subjected to the M-HCC model showed an important elevation in the protein level of IL-1β ($p = 0.0001$), IL-18 ($p = 0.0001$), and p65 ($p = 0.0031$); of note, NAR treatment attenuated these increments (IL-1β, $p = 0.0001$; IL-18, $p = 0.0001$; and p65, $p = 0.0035$). M-HCC model also decreased ($p = 0.0001$) peroxisome proliferator-activated receptor gamma (PPAR-γ) protein level (Fig. 3h) but increased ($p = 0.0014$) sterol regulatory element-binding protein 1C (SREBP-1C) (Fig. 3i).

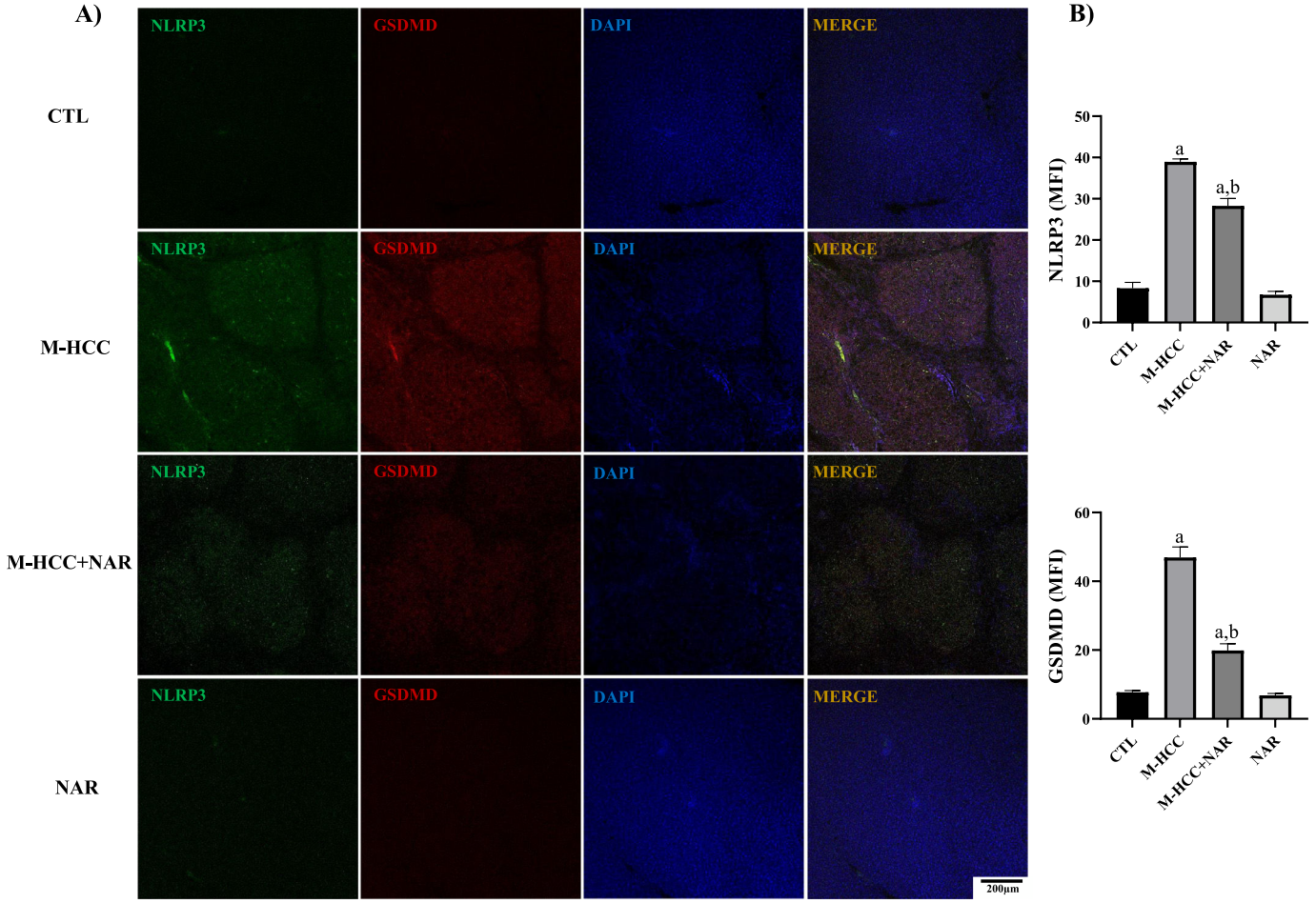

Fig. 5. Effect of NAR on NLRP3 inflammasome and pyroptosis activation.

(A) IF analysis of NLRP3-GSDMD. **(B)** Quantification of NLRP3 and GSDMD fluorescence density (MFI). In plots, bars represent the mean ± SEM obtained by two-way ANOVA statistical analysis. Statistically significant when compared with CTL (a) and M-HCC (b) groups; $p < 0.05$. control; M-HCC, MASH-driven HCC; NAR, naringenin; M-HCC+NAR, MASH-driven HCC administrated with naringenin. $n = 3$ animals per group. Magnification is 10×.

Interestingly, NAR treatment attenuated these alterations (SREBP-1C, $p = 0.0161$; PPAR-γ, $p = 0.0061$), as compared with animals subjected only to the M-HCC model. NAR alone did not affect these parameters.

3.3. NAR inhibits the NLRP3 inflammasome/pyroptosis pathway

The percentages of NLRP3-, caspase-1-, and GSDMD-positive areas in the livers of the control animals are shown in (Fig. 4a). Rats in the M-HCC model exhibited increased ($p = 0.0001$) levels of these proteins (Fig. 4b). Western blot analysis (Fig. 4c,d,e) validated this evidence (NLRP3, $p = 0.0004$; caspase-1, $p = 0.0021$; and GSDMD-N, $p = 0.0002$); however, pro-caspase-1 protein levels were not altered in any group (Fig. 4f). Nevertheless, NAR administration blocked NLRP3 inflammasome ($p = 0.0033$); caspase-1 ($p = 0.0661$), GSDMD-N ($p = 0.0021$), and NLRP3 inflammasome/pyroptosis activation in the livers of rats in the M-HCC model. The NLRP3/pyroptosis signaling pathway remained unchanged following NAR treatment.

To assess the effect of NAR treatment on pyroptosis activation, we detected NLRP3 and GSDMD proteins by IF analysis (Fig. 5). The results showed that the M-HCC model had increased levels of NLRP3 ($p = 0.0001$) and GSDMD ($p = 0.0001$) protein in altered hepatocyte foci. Conversely, NAR administration reduced (NLRP3, $p = 0.0031$; and GSDMD, $p = 0.0013$) the levels of these proteins (Fig. 5a), and quantitative analysis corroborated this observation (Fig. 5b). NAR and control groups did not affect protein levels.

3.4. NAR reduced collagen content, stellate cell activation, and fibrosis

The percentage of the collagen content-positive area increased in the livers of animals subjected to the M-HCC model, whereas NAR administration reduced ($p = 0.0001$) this content (Fig. 6a,b). Moreover, ECM accumulation was corroborated by quantifying hydroxyproline levels in liver samples, which showed that it was increased ($p = 0.0010$) in the M-HCC model compared to controls. In contrast, the NAR treatment reduced this effect ($p = 0.0248$). However, the NAR alone did not affect this parameter (Fig. 6c).

Stellate cell activation is considered a profibrogenic event, therefore presence of activation markers TGF-β and alpha-smooth muscle actin (α-SMA) was evaluated. Western blot analysis revealed that the M-HCC model increased TGF-β ($p = 0.0005$) and α-SMA ($p = 0.0004$) protein levels as compared with controls, NAR treatment partially reduced ($p = 0.0125$ and $p = 0.0055$, respectively) the level of these proteins (Fig. 6d,e). However, the NAR alone did not affect these levels.

3.5. NAR prevents the preneoplastic lesions' appearance and cell proliferation in early hepatocarcinogenesis

The livers of the M-HCC model developed nodules and tumors, as detected by GGT activity and glutathione S-transferase pi 1 (GSTP1) levels, two HCC markers, and the level of KI67, a proliferation marker

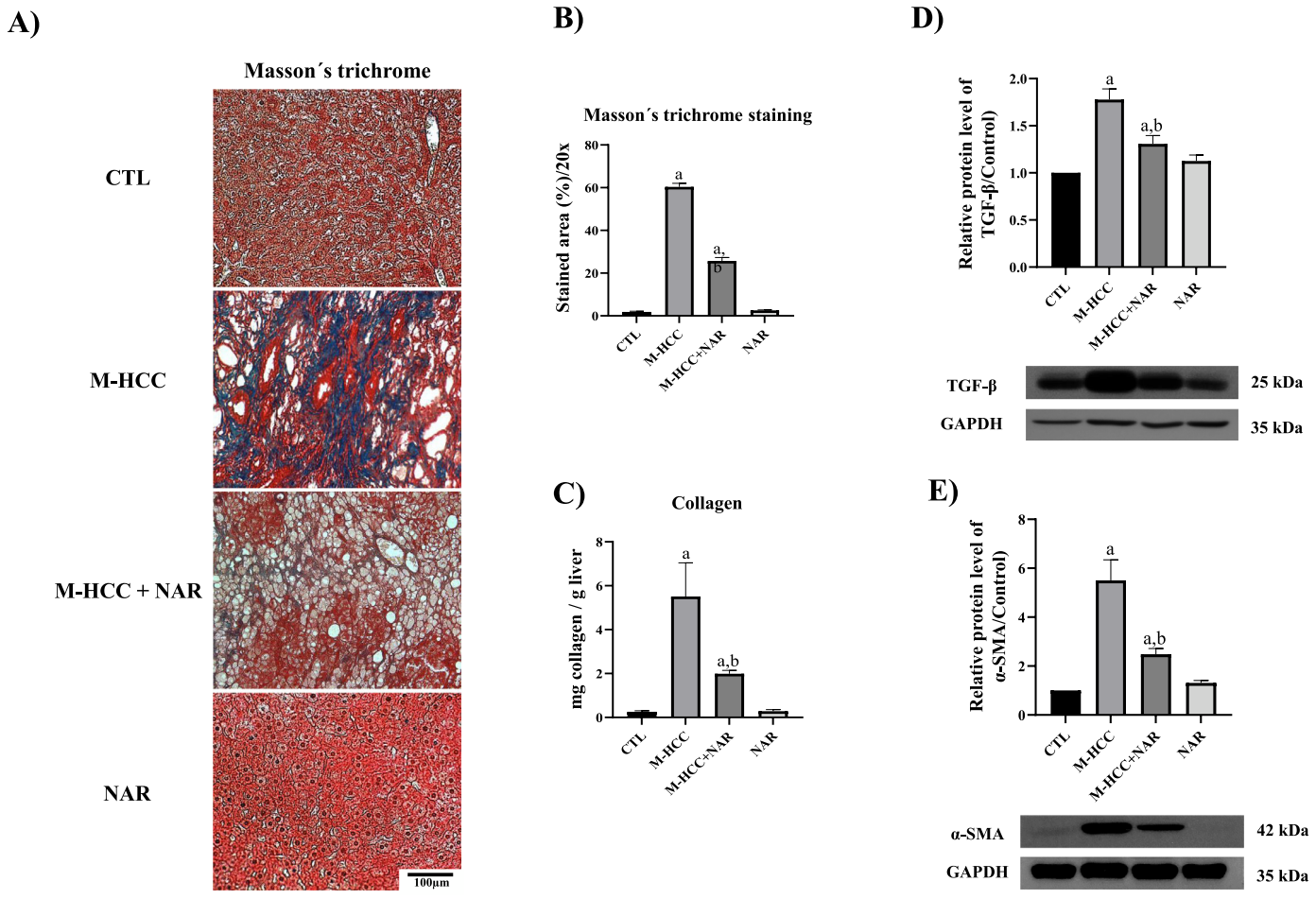

Fig. 6. Effect of NAR on fibrosis and profibrogenic mediators.

(A) Representative images of Masson's trichrome staining. Scale bars represent = 100 μm. **(B)** Percentage of collagen area ($n = 3$). **(C)** Collagen content was determined by measuring the liver hydroxyproline level ($n = 5$). Western blot analysis of TGF-β ($n = 3$) (**D**), α-SMA ($n = 3$) (**E**). The protein level of interest was normalized to that of GAPDH used as the loading control. In plots, bars represent the mean ± SEM obtained by two-way ANOVA statistical analysis. Statistically significant when compared with CTL (a) and M-HCC (b) groups; $p < 0.05$. control; M-HCC, MASH-driven HCC; NAR, naringenin; M-HCC+NAR, MASH-driven HCC administrated with naringenin.

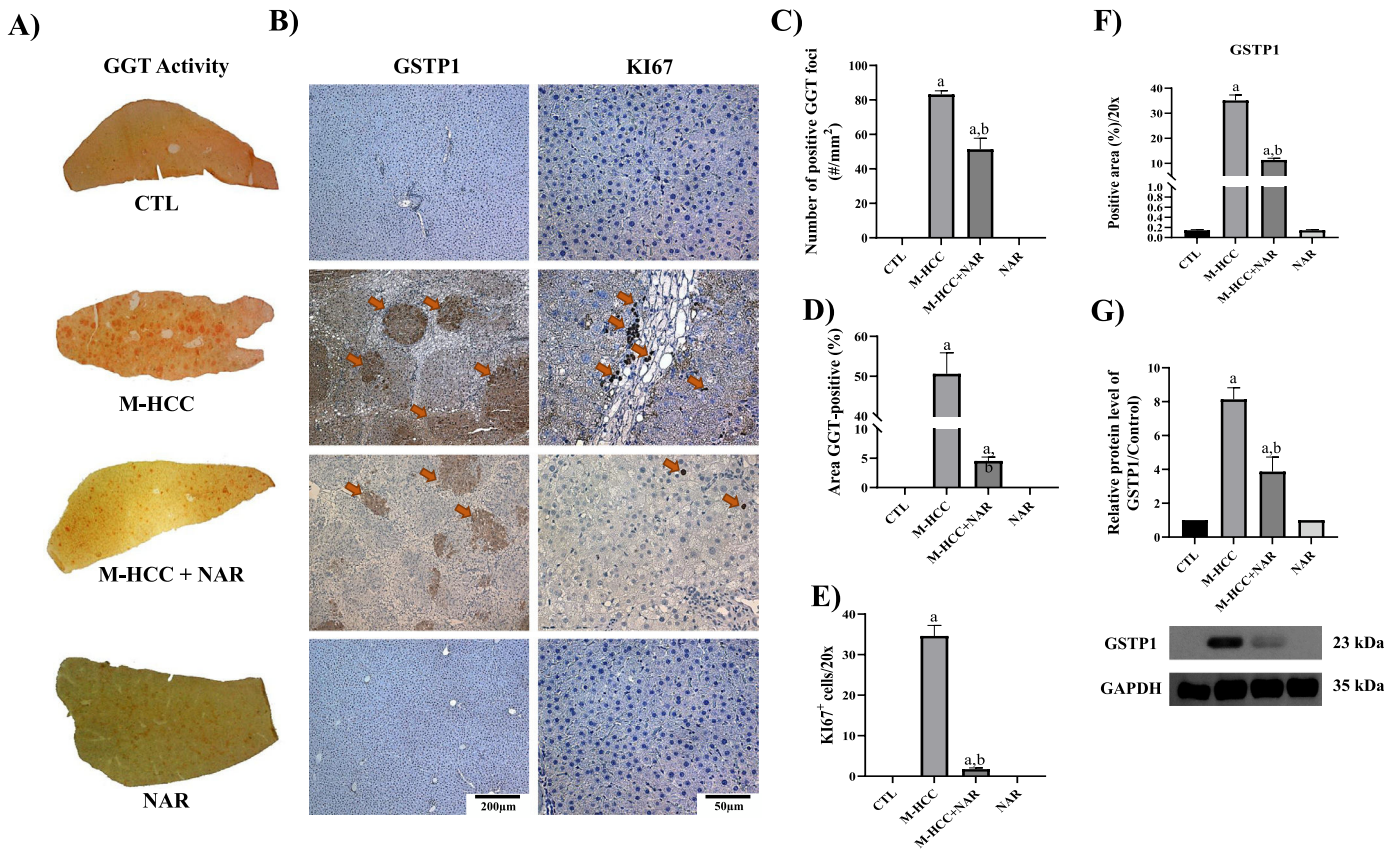

Fig. 7. Effect of NAR on fibrosis and preneoplastic lesion development.

(A) Macroscopic images of liver sections showing preneoplastic lesions detected by GGT activity (n = 5). **(B)** IHC staining of GSTP1 and KI67 proteins, and Masson's trichrome staining (n = 3). **(C)** Number of GGT-positive foci. **(D)** Percentage of GGT-positive area. **(E)** Plot of KI67-positive nuclei quantification. **(F)** Quantification of GSTP1-positive area. **(G)** Protein level GSTP1 by Western blot. In plots, bars represent the mean ± SEM obtained by two-way ANOVA statistical analysis. Statistically significant when compared with CTL (a) and M-HCC (b) groups; $p < 0.05$. control; M-HCC, MASH-driven HCC; NAR, naringenin; M-HCC+NAR, MASH-driven HCC administrated with naringenin.

(Fig. 7a,b,c). These proteins were strongly induced in the livers of animals in the MASH—HCC model. The GSTP1-positive area increased >30-fold (p =0.0001), and the number of KI67-positive cells increased (p = 0.0001) in the M-HCC model.

In addition, the number of GGT-positive foci increased 86-fold (p = 0.0001) in M-HCC animals compared to that in controls; however, NAR treatment decreased (p = 0.0001) this number by 35 %. Similarly, the percentage of GGT-positive areas increased (p = 0.0001) in the M-HCC model; however, NAR treatment reduced (p = 0.0001) this percentage (Fig. 7d). Notably, NAR treatment strongly prevented (p = 0.0001) KI67 and GSTP1 levels (Fig. 7e,f). Increased (p = 0.0001) GSTP1 levels in M-HCC animals were corroborated by western blot analysis. In contrast, NAR administration prevented this increase (p = 0.0025; Fig. 7g).

3.6. Docking analysis identifies potential interactions of NAR with possible therapeutic targets involved in the early HCC promoted by mash

Fig. 8 shows the binding affinity assays of NAR with NF-κB, IL-1β, IL-18, NLRP3, caspase-1, ASC, GSDMD, P2×7R, TXNIP, and ChREBP protein. Results indicated that NAR showed medium binding energy of −6.46 kcal/mol. The main interaction of NAR with NF-κB was with ASP215, LEU218, ILE219, LYS122, ILE46, and GLY48 amino acids, with a binding energy of −7.2 kcal/mol (Fig. 8a), IL-1β, and IL-18 presented a binding energy of −6.6 and −2.9 kcal/mol, respectively (Fig. 8b,c). IL-1β interacted with NAR through TYR24, LEU82, LEU80, and PRO78 amino acids and IL-18 through ARG104 and GLU116 residues.

Molecular docking between NLRP3 and NAR shows a medium binding energy of −8.2 kcal/mol and interacts with TYR443, ILE411, ALA227, ARG578, TYR632, and ASP662 residues (Fig. 8d). The docked energy of NAR with caspase-1 was −6.5 kcal/mol interacting with HIS237, GLN283, ALA284, ARG341, and CYS285 residues (Fig. 8e). Moreover, docking between ASC and NAR was −4.9 kcal/mol and interacted with PHE163, LEU192, LEU178, and LYS174 amino acids (Fig. 8f), and GSDMD showed a binding energy of −6.7 kcal/mol interacting with LEU49, PRO73, ASP47 and ALA53 residues (Fig. 8g).

The P2×7R docking energy with NAR was −8.3 kcal/mol interacting with ARG256, GLN195, TYR105, ASN191, VAL102, VAL190, CYS194, ASN159, PHE106, and SER156 amino acids (Fig. 8h). The binding energy of TXNIP protein was −6.6 kcal/mol interacting with TYR99, VAL89, ALA43, and GLU85 residues (Fig. 8i), and the affinity energy of NAR with ChERBP was −6.6 kcal/mol interacting with LEU174, ARG128, ARG129, ARG58 and TRP127 amino acids (Fig. 8j). The corresponding binding energies are presented in Table 3.

4. Discussion

In recent decades, the obesity epidemic has led to an increase in liver transplantation in MASH-associated HCC and is currently the second leading cause of liver transplantation in humans [31,32]. However, a lack of sufficient donors, liver rejection, and elevated costs render this procedure unsuitable for most patients [31]. Unfortunately, there are currently no effective pharmacological treatments for MASH-driven HCC. In this study, we found that NAR administration inhibited the pro-inflammatory NLRP3/pyroptosis pathway, profibrogenic TGF-β factor, and HSC activation, leading to the attenuation of inflammation and fibrosis. Moreover, NAR reduced GGT and GSTP1 levels and prevented an increase in the expression of

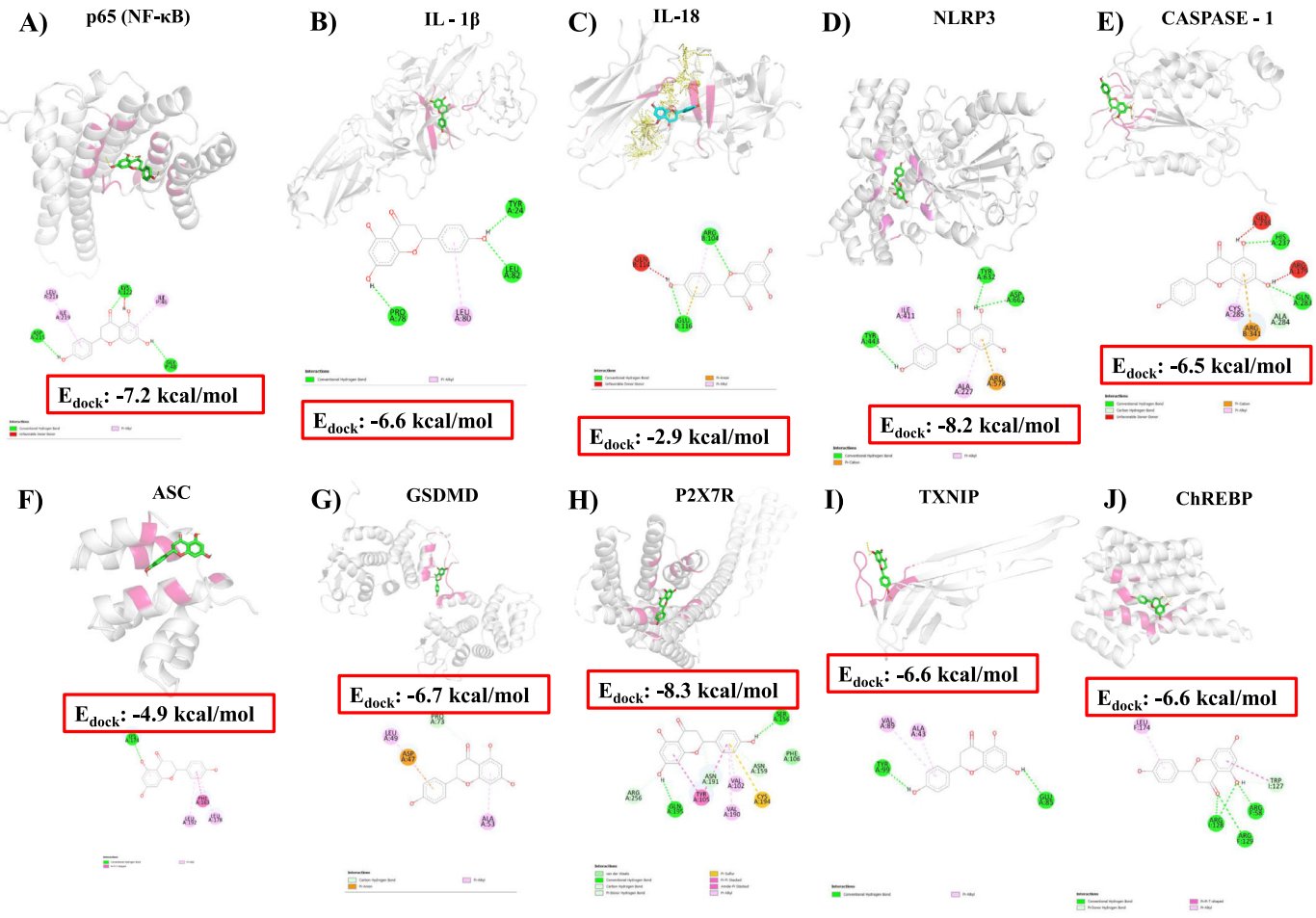

Fig. 8. Molecular docking and binding energy of NAR with proteins involved in the NLRP3 inflammasome/pyroptosis pathway.

Molecular docking of naringenin (NAR) illustrates the interaction of amino acids and binding energy with NF-κB p65 **(A)**, IL-1β **(B)**, IL-18 **(C)**, NLRP3 **(D)**, caspase-1 **(E)**, ASC **(F)**, GSDMD **(G)**, P2×7R **(H)**, TXNIP **(I)**, ChREBP **(J)** proteins.

the proliferation marker KI67. Notably, NAR treatment completely prevented the appearance of tumors in animals subjected to the M-HCC model. Therefore, our findings show that NAR inhibits the progression of MASH to HCC. Nevertheless, further basic and clinical research on the use of NAR in treating human MASH-driven HCC is imperative.

HCC typically develops during chronic liver inflammation, and the NLRP3 inflammasome/pyroptosis pathway plays a pivotal role in the inflammatory onset [33]. Similarly, MASH exacerbates the activation of this pathway, thereby generating harmful lipid compounds and increasing intestinal membrane permeability [9]. This leads to the release of pathogen-associated molecular patterns (PAMPs) or DAMPs, which are crucial for the assembly of NLRP3 active oligomers [34,35]. Extensive evidence has shown that during MASH, PAMPs or DAMPs bind to toll-like receptors on the cell membrane and trigger the activation of NF-κB signaling pathways, which are pivotal inflammatory factors in HCC progression [32,36]. This activation leads to the transcription of inflammasome components such as NLRP3, pro-IL-1β, and pro-IL-18, thereby perpetuating inflammation [36]. Oxidative stress also promotes the assembly of active NLRP3 oligomers by activating P2×7R or TXNIP, which leads to caspase-1 activation [33]. Upon activation, caspase-1 cleaves GSDMD at its N-terminus to convert pro-IL-1β and pro-IL-18 into their mature forms, namely IL-1β and IL-18, respectively [33,36]. Thus, the NLRP3 inflammasome/pyroptosis pathway is a potent promoter of inflammation and contributes to HCC progression [33,36]. Both the NLRP3 inflammasome and GSDMD must be in an oxidized state to exhibit activity, thereby underscoring the crucial role of reactive oxygen species in the regulation of this pathway [33,36,37].

Based on our M-HCC model, our research confirms that activation of the NLRP3 inflammasome/pyroptosis signaling pathway is crucial in the progression of HCC from MASH. We observed increased levels of NLRP3, caspase-1, and GSDMD proteins in our model, which consequently magnified IL-1β, and IL-18 production and release, and promoted inflammation and fibrosis. Importantly, our results suggest that the NLRP3 inflammasome contributes to the pathogenesis of HCC by increasing the metabolic activity and proliferation of cancerous cells.

In contrast, NAR, a trihydroxy flavanone found abundantly in fruits such as oranges, pomelos, grapefruits, tomatoes, fenugreek, and coffee, possesses diverse pharmacological and biological effects that are beneficial for human health, including antioxidant, anticancer, anti-inflammatory, antifungal, and antimicrobial properties [12,38]. Our previous studies have demonstrated the effectiveness of a 100 mg/kg NAR dose at mitigating inflammation and fibrosis in a liver damage model induced by CCl_4; therefore, we used the same dose to investigate the pharmacological effect of NAR on MASH—HCC progression [12]. Our findings indicate that NAR exhibits anti-inflammatory and anticancer properties that counteract fat accumulation, inflammation, and fibrosis, thereby suggesting that the beneficial effects of NAR stem from its ability to regulate lipid metabolism and inhibit the NLRP3 inflammasome/pyroptosis pathway. These results align with previous research thereby demonstrating the capability of NAR to deactivate the NLRP3 pathway via AhR in pancreatitis-linked

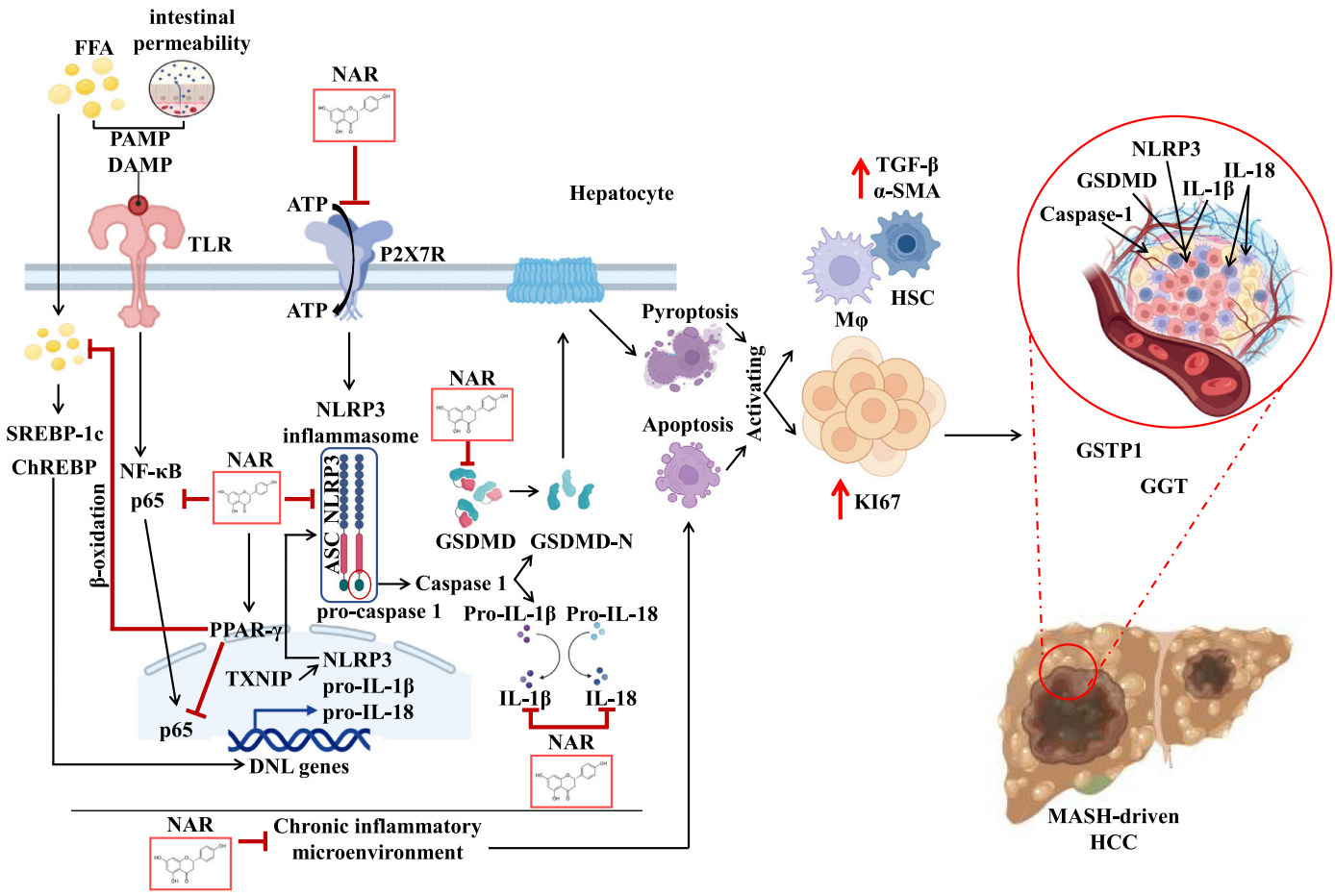

Fig. 9. NAR attenuates MASH-driven HCC by modulating chronic inflammatory microenvironment and cell proliferation.

This illustration depicts the possible molecular pathways by which NAR prevents MASH-driven HCC. The MASH—HCC model triggers the release of PAMPs, such as lipopolysaccharides, and DAMPs, such as ATP. The DAMPs and PAMPs bind to TLR reducing PPAR-γ and activating SREBP-1c, ChREBP, and subsequently, the NF-κB pathway. This pathway upregulates NLRP3, IL-1β and IL-18. Molecular docking suggests that NAR interacts with NF-κB, reducing NLRP3, pro-IL-1β, and pro-IL-18 transcription. Moreover, NAR binds to P2×7R and TXNIP inhibiting NLRP3, ASC, and pro-caspase-1 oligomerization. NAR may block NLRP3 inflammasome activation, reducing activation of interleukin active forms, and preventing GSDMD pore formation, thereby averting pyroptosis. A chronic inflammatory environment triggered by NLRP3 inflammasome activation also promotes apoptosis. Both pyroptosis and apoptosis stimulate macrophages and the production of TGF-β profibrogenic factor, which activates HSC to produce α-SMA, contributing to fibrosis. Additionally, prolonged injury triggers compensatory cell proliferation, characterized by increased KI67 levels, which leads to the formation of GGT and GSTP1-positive, culminating in HCC development.

intestinal injury [39]. Similarly, was elucidated the NAR suppression effect on NLRP3 inflammasome activation via the mRNA-208a signaling pathway in isoproterenol-induced myocardial infarction [40].

Our study revealed that NAR not only diminished NLRP3 inflammasome pathway activation but also reduced GSDMD formation, thereby impeding pyroptosis. We propose that NAR functions as a multitarget drug to prevent MASH. Firstly, by lowering NLRP3 and NF-κB p65 protein level, and secondly, by interacting with NF-κB p65, thereby impeding its translocation into cell nuclei and mitigating subsequent transcription of NLRP3, pro-IL-1β, and pro-IL-18. Additionally, NAR exhibited potent anticancer effects by reducing KI67, GGT, and GSTP1 levels; these are well-known markers associated with cell proliferation and hepatocarcinogenesis [41]. This suggests that NAR has additional mechanisms of action against MASH—HCC progression, in addition to inhibition of the NLRP3 inflammasome/pyroptosis signaling pathway.

Docking results suggest that NAR may produce hepatoprotective effects through molecular interactions with NF-κB p65, NLRP3, ASC, caspase-1, IL-1β, IL-18, and GSDMD; furthermore, it revealed that NAR exhibits an affinity for TXNIP, P2×7R, and ChREBP, which supports its potential to attenuate NLRP3 inflammasome activation via non-canonical pathways. However, further studies are required to confirm these hypotheses.

5. Conclusions

Our study highlighted the anti-steatotic, anti-inflammatory, anti-fibrotic, and anti-neoplastic properties of NAR in the early progression of HCC promoted by MASH while also offering a promising avenue for the treatment of this pathology. This therapeutic effect is closely associated with the inhibition of SREBP-1C, PPAR-γ, NLRP3 inflammasome, GSDMD, TGF-β, HSC, GGT, GSTP1, and KI67 (Fig. 9). Moreover, given the safety profile of NAR, our findings strongly support its use in treating MASH-driven HCC in humans. However, further investigations using both fundamental and clinical approaches are warranted to unravel the supplementary mechanisms underlying the molecular players implicated in the evolution from MASH to HCC. Additional basic and clinical studies are needed before NAR can be prescribed as a treatment for MASH-driven HCC.

Author contributions

All authors have read and agreed to the published version of the manuscript.

Declaration of interests

None.

CRediT authorship contribution statement

Linda Vanessa Márquez-Quiroga: Conceptualization, Methodology, Software, Formal analysis, Investigation, Writing – original draft, Writing – review & editing. **Aline Barboza-López:** Methodology. **Jose Y. Suárez-Castillo:** Methodology. **Irina Cardoso-Lezama:** Methodology, Software. **Miguel Á. Fuentes-Figueroa:** Methodology, Software. **Eduardo E. Vargas-Pozada:** Methodology. **Juan D. Rodriguez-Callejas:** Methodology, Software. **Erika Ramos-Tovar:** Writing – original draft, Writing – review & editing. **Carolina Piña-Vázquez:** Writing – original draft, Writing – review & editing. **Jaime Arellanes-Robledo:** Writing – original draft, Writing – review & editing, Funding acquisition. **Saúl Villa-Treviño:** Writing – original draft, Writing – review & editing, Funding acquisition. **Pablo Muriel:** Conceptualization, Formal analysis, Investigation, Writing – original draft, Writing – review & editing, Supervision, Project administration, Funding acquisition.

Funding

This work was supported by the National Council of Humanities, Science, and Technology (Conahcyt) of Mexico (grant no. CF2019 –53358 to S.V.-T, J.A.-R. and P.M., and fellowship no. 814088 to L.V. M.-Q.).

Acknowledgments

We thank Rosa E. Flores-Beltrán, Laura Dayana Buendia-Montaño, Rafael Leyva, Benjamin E. Chavez, and Iván J. Galván Mendoza for technical assistance and for providing the necessary instrumentation and Jorge Fernández-Hernández for giving us animal laboratory facilities.

Data availability statement

All data produced or analyzed are included in the article.

References

[1] Platek AE, Szymanska A. Metabolic dysfunction-associated steatotic liver disease as a cardiovascular risk factor. Clin Exp Hepatol 2023;9(3):187–92. https://doi.org/10.5114/ceh.2023.130744.
[2] Kneeman JM, Misdraji J, Corey KE. Secondary causes of nonalcoholic fatty liver disease. Therap adv Gastroenterol 2012;5(3):199–207. https://doi.org/10.1177/1756283×11430859.
[3] Rinella ME, Lazarus JV, Ratziu V, Francque SM, Sanyal AJ, Kanwal F, et al. A multisociety Delphi consensus statement on new fatty liver disease nomenclature. Ann Hepatol 2024;29(1):101133. https://doi.org/10.1016/j.aohep.2023.101133.
[4] Phoolchund AGS, Khakoo SI. MASLD and the development of HCC: pathogenesis and therapeutic challenges. Cancers (Basel) 2024;6(2):259. 16. https://doi.org/10.3390/cancers16020259.
[5] Márquez-Quiroga LV, Arellanes-Robledo J, Vásquez-Garzón VR, Villa-Treviño S, Muriel P. Models of nonalcoholic steatohepatitis potentiated by chemical inducers leading to hepatocellular carcinoma. Biochem Pharmacol 2012;195:114845. https://doi.org/10.1016/j.bcp.2021.114845.
[6] Tang YL, Tao Y, Zhu L, Shen JL, Cheng H. Role of NLRP3 inflammasome in hepatocellular carcinoma: a double-edged sword. Int Immunopharmacol 2023;118:110107. https://doi.org/10.1016/j.intimp.2023.110107.
[7] Zhao H, Zhang Y, Zhang Y, Chen C, Liu H, Yang Y, Wang H. The role of NLRP3 inflammasome in hepatocellular carcinoma. Front Pharmacol 2023;14:1150325. https://doi.org/10.3389/fphar.2023.1150325.
[8] Cardoso-Lezama I, Fuentes-Figueroa MÁ, Ramos-Tovar E, Márquez-Quiroga LV, Ortiz-Fernández A, Vargas-Pozada E, et al. Nicotinic acid attenuates experimental non-alcoholic steatohepatitis by inhibiting the NLRP3 inflammasome/pyroptosis pathway. Biochem Pharmacol 2023;216:115762. https://doi.org/10.1016/j.bcp.2023.115762.
[9] Ramos-Tovar E, Muriel P. NLRP3 inflammasome in hepatic diseases: a pharmacological target. Biochem Pharmacol 2023;217:115861. https://doi.org/10.1016/j.bcp.2023.115861.
[10] Pinter M, Pinato DJ, Ramadori P, Heikenwalder M. N.ASH and hepatocellular carcinoma: immunology and immunotherapy. Clin Cancer Res 2023;29(3):513–20. https://doi.org/10.1158/1078-0432.CCR-21-1258.
[11] Mao F, Wang E, Fu L, Fan W, Zhou J, Yan G, et al. Identification of pyroptosis-related gene signature in nonalcoholic steatohepatitis. Sci Rep 2024;14(1):3175. https://doi.org/10.1038/s41598-024-53599-8.
[12] Hernández-Aquino E, Zarco N, Casas-Grajales S, Ramos-Tovar E, Flores-Beltrán RE, Arauz J, et al. Naringenin prevents experimental liver fibrosis by blocking tgfβ-Smad3 and JNK-Smad3 pathways. World J Gastroenterol 2017;23(24):4354–68. https://doi.org/10.3748/wjg.v23.i24.4354.
[13] Hernández-Aquino E, Muriel P. Beneficial effects of naringenin in liver diseases: molecular mechanisms. World J Gastroenterol 2018;24(16):1679–707. https://doi.org/10.3748/wjg.v24.i16.1679.
[14] Wang Q, Ou Y, Hu G, Wen C, Yue S, Chen C, et al. Naringenin attenuates non-alcoholic fatty liver disease by down-regulating the NLRP3/NF-κb pathway in mice. Br J Pharmacol 2020;177(8):1806–21. https://doi.org/10.1111/bph.14938.
[15] Faramarzi F, Alimohammadi M, Rahimi A, Alizadeh-Navaei R, Shakib RJ, Rafiei A. Naringenin induces intrinsic and extrinsic apoptotic signaling pathways in cancer cells: a systematic review and meta-analysis of in vitro and in vivo data. Nutr Res 2022;105:33–52. https://doi.org/10.1016/j.nutres.2022.05.003.
[16] Matsuda H, Chisaka T, Kubomura Y, Yamahara J, Sawada T, Fujimura H, Kimura H. Effects of crude drugs on experimental hypercholesterolemia. I. Tea and its active principles. J Ethnopharmacol 1986;17(3):213–24. https://doi.org/10.1016/0378-8741(86)90138-8.
[17] Vargas-Pozada EE, Ramos-Tovar E, Acero-Hernández C, Cardoso-Lezama I, Galindo-Gómez S, Tsutsumi V, Muriel P. Caffeine mitigates experimental nonalcoholic steatohepatitis and the progression of thioacetamide-induced liver fibrosis by blocking the MAPK and TGF-β/Smad3 signaling pathways. Ann Hepatol 2022;27(2):100671. https://doi.org/10.1016/j.aohep.2022.100671.
[18] Vargas-Pozada EE, Ramos-Tovar E, Rodriguez-Callejas JD, Cardoso-Lezama I, Galindo-Gómez S, Gil-Becerril K, et al. Activation of the NLRP3 inflammasome by CCl4 exacerbates hepatopathogenic diet-induced experimental NASH. Ann Hepatol 2023;28(1):100780. https://doi.org/10.1016/j.aohep.2022.100780.
[19] Schiffer E, Housset C, Cacheux W, Wendum D, Desbois-Mouthon C, Rey C, et al. Gefitinib, an EGFR inhibitor, prevents hepatocellular carcinoma development in the rat liver with cirrhosis. Hepatology 2005;1(2):307–14. https://doi.org/10.1002/hep.20538.
[20] Reitman S, Frankel S. A colorimetric method for the determination of serum glutamic oxalacetic and glutamic pyruvic transaminases. Am J Clin Pathol 1957;28(1):56–63. https://doi.org/10.1093/ajcp/28.1.56.
[21] Bessey OA, Lowry OH, Brock MJ. A method for the rapid determination of alkaline phosphates with five cubic millimeters of serum. J Biol Chem 1946;164:321–9.
[22] Glossmann H, Neville DM. gamma-glutamyltransferase in kidney brush border membranes. FEBS Lett. 1972;19(4):340–4. https://doi.org/10.1016/0014-5793(72)80075-9.
[23] Seifter S, Dayton S. The estimation of glycogen with the anthrone reagent. Arch Biochem 1950;25(1):191–200.
[24] Arellanes-Robledo J, Reyes-Gordillo K, Ibrahim J, Leckey L, Shah R, Lakshman MR. Ethanol targets nucleoredoxin/dishevelled interactions and stimulates phosphatidylinositol 4-phosphate production in vivo and in vitro. Biochem Pharmacol 2018;156:135–46. https://doi.org/10.1016/j.bcp.2018.08.021.
[25] Smith PK, Krohn RI, Hermanson GT, Mallia AK, Gartner FH, Provenzano MD, et al. Measurement of protein using bicinchoninic acid. Anal Biochem 1985;150(1):76–85. https://doi.org/10.1016/0003-2697(85)90442-7.
[26] López-Torres CD, Torres-Mena JE, Castro-Gil MP, Villa-Treviño S, Arellanes-Robledo J, Del Pozo-Yauner L, et al. Downregulation of indolethylamine N-methyltransferase is an early event in the rat hepatocarcinogenesis and is associated with poor prognosis in hepatocellular carcinoma patients. J Gene Med 2022;24(8):e3439. https://doi.org/10.1002/jgm.3439.
[27] Rodriguez-Callejas JD, Fuchs E, Perez-Cruz C. Increased oxidative stress, hyperphosphorylation of tau, and dystrophic microglia in the hippocampus of aged Tupaia belangeri. Glia 2020;68(9):1775–93. https://doi.org/10.1002/glia.23804.
[28] Mehlem A, Hagberg CE, Muhl L, Eriksson U, Falkevall A. Imaging of neutral lipids by oil red O for analyzing the metabolic status in health and disease. Nat Protoc 2013;8(6):1149–54. https://doi.org/10.1038/nprot.2013.055.
[29] Piña R, Santos-Díaz AI, Orta-Salazar E, Aguilar-Vazquez AR, Mantellero CA, Acosta-Galeana I, et al. Ten approaches that improve immunostaining: a review of the latest advances for the optimization of immunofluorescence. Int J Mol Sci 2022;23(3):1426. https://doi.org/10.3390/ijms23031426.
[30] Chandrakala C, Sravanthi P, Raj Bharath S, Arockiasamy S, George Johnson M, Nagaraja KS, et al. Synthesis, structure, vapour pressure and deposition of ZnO thin film by plasma assisted MOCVD technique using a novel precursor bis[(pentylnitrilomethylidine) (pentylnitrilomethylidine-μ-phenalato)]dizinc(II). J Mol Struct 2017;1130:1–9. https://doi.org/10.1016/j.molstruc.2016.10.010.
[31] Burra P, Becchetti C, Germani G. NAFLD and liver transplantation: disease burden, current management and future challenges. JHEP Rep 2020;2(6):100192. https://doi.org/10.1016/j.jhepr.2020.100192.
[32] Holzner ML, Florman S, Schwartz ME, Tabrizian P. Outcomes of liver transplantation for nonalcoholic steatohepatitis-associated hepatocellular carcinoma. HPB 2022;24(4):470–7. https://doi.org/10.1016/j.hpb.2021.08.943.
[33] Hurtado-Navarro L, Angosto-Bazarra D, Pelegrín P, Baroja-Mazo A, Cueva S. NLRP3 Inflammasome and pyroptosis in liver pathophysiology: the emerging relevance of Nrf2 inducers. Antioxidants (Basel) 2022;11(5):870. https://doi.org/10.3390/antiox11050870.
[34] Ganz M, Szabo G. Immune and inflammatory pathways in NASH. Hepatol Int 2013;7(Suppl 2):771–81 Suppl 2. https://doi.org/10.1007/s12072-013-9468-6.

[35] Lucas-Ruiz F, Peñín-Franch A, Pons JA, Ramírez P, Pelegrín P, Cuevas S, et al. Emerging role of NLRP3 inflammasome and pyroptosis in liver transplantation. Int J Mol Sci 2022;23(22):14396. https://doi.org/10.3390/ijms232214396.
[36] Toldo S, Abbate A. The role of the NLRP3 inflammasome and pyroptosis in cardiovascular diseases. Nat Rev Cardiol 2024;21(4):219–37. https://doi.org/10.1038/s41569-023-00946-3.
[37] Wree A, Eguchi A, McGeough MD, Pena CA, Johnson CD, Canbay A. NLRP3 inflammasome activation results in hepatocyte pyroptosis, liver inflammation, and fibrosis in mice. Hepatology 2014;59(3):898–910. https://doi.org/10.1002/hep.26592.
[38] Duda-Madej A, Stecko J, Sobieraj J, Szymańska N, Kozłowska J. Naringenin and its derivatives-health-promoting phytobiotic against resistant bacteria and fungi in humans. Antibiotics (Basel) 2022;11(11):1628. https://doi.org/10.3390/antibiotics11111628.
[39] Yan X, Lin T, Zhu Q, Zhang Y, Song Z, Pan X. Naringenin protects against acute pancreatitis-associated intestinal injury by inhibiting NLRP3 inflammasome activation via AhR signaling. Front Pharmacol 2023;14:1090261. https://doi.org/10.3389/fphar.2023.1090261.
[40] Eldourghamy A, Hossam T, Hussein MA, Abdel-Aziz A, El-masry SA. Naringenin suppresses NLRP3 inflammasome activation via the mRNA-208a signaling pathway in isoproterenol-induced myocardial infarction. Asian Pac J Trop Biomed 2023;13(10). https://doi.org/10.4103/2221-1691.387750.
[41] Fuentes-Hernández S, Alarcón-Sánchez BR, Guerrero-Escalera D, Montes-Aparicio AV, Castro-Gil MP, Idelfonso-García OG, Rosas-Madrigal S, et al. Chronic administration of diethylnitrosamine to induce hepatocarcinogenesis and to evaluate its synergistic effect with other hepatotoxins in mice. Toxicol Appl Pharmacol 2019;378:114611. https://doi.org/10.1016/j.taap.2019.114611.